

# HDR Environment Map Estimation for Real-Time Augmented Reality

GOWRI SOMANATH, Apple Inc.  
DANIEL KURZ, Apple Inc.

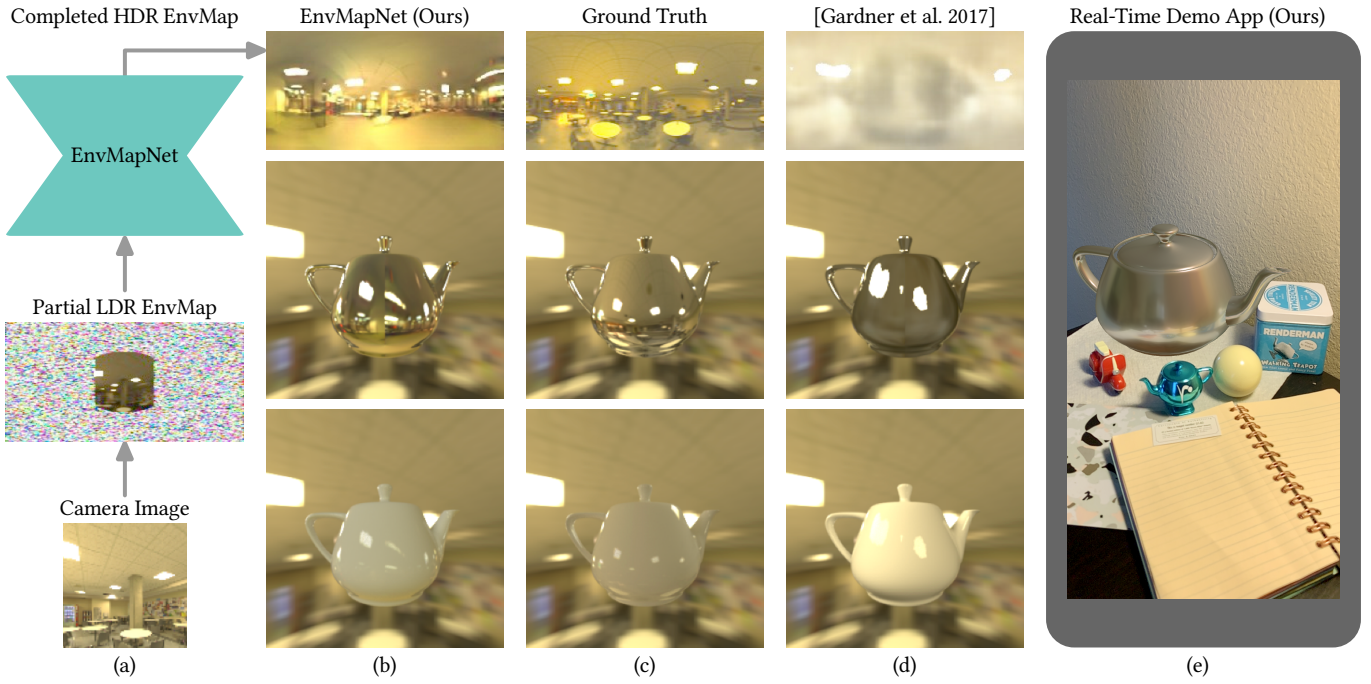


Fig. 1. Given a partial LDR environment map from a camera image, we estimate a visually coherent and completed HDR environment map (a), that can be used by graphics engines to create light and reflection probes. These enable rendering virtual objects with any material finish into the real environment in a perceptually pleasing and realistic way (b), more similar to ground truth (c) than state-of-the-art methods (d). Our mobile app renders a virtual metallic teapot with 0.2 roughness, using our estimated environment map in real-time (e). **We refer to the supplementary material for more results and videos.**

We present a method to estimate an HDR environment map from a narrow field-of-view LDR camera image in real-time. This enables perceptually appealing reflections and shading on virtual objects of any material finish, from mirror to diffuse, rendered into a real physical environment using augmented reality. Our method is based on our efficient convolutional neural network architecture, EnvMapNet, trained end-to-end with two novel losses, ProjectionLoss for the generated image, and ClusterLoss for adversarial training. Through qualitative and quantitative comparison to state-of-the-art methods, we demonstrate that our algorithm reduces the directional error of estimated light sources by more than 50%, and achieves 3.7 times lower Frechet Inception Distance (FID). We further showcase a mobile application that is able to run our neural network model in under 9 ms on an iPhone XS, and render in real-time, visually coherent virtual objects in previously unseen real-world environments.

Additional Key Words and Phrases: Augmented Reality, Scene Completion, Environment Map Estimation, Image Based Lighting

## 1 INTRODUCTION

In this work, we discuss video see-through augmented reality (AR) applications, in which virtual objects are superimposed on a camera image of the real (physical) environment shown on an opaque display, e.g. on a phone as shown in Figure 1(e). Creating immersive and believable AR experiences involves many aspects of computer vision and computer graphics. One of the requirements is visual coherence: the problem of matching visual appearance of rendered virtual objects to their real-world background, such that rendered and real objects become indistinguishable in the composited video stream. Accomplishing this involves matching various scene and camera properties, such as lighting, geometry, and sensor noise.

This paper focusses on creating reflections and lighting effects for virtual objects, by estimating an omnidirectional HDR environment map, also commonly referred to as IBL from its use in Image Based Lighting. To support rendering virtual objects with a variety of geometry, material properties, and dimensions, the environment map must be high dynamic range, and have sufficient image resolution to represent objects and features in the scene. We use the equirectangular projection and RGB color space to represent the environment maps. As shown in Figure 1(a), the core challenge in

Authors' addresses: Gowri Somanath, Apple Inc., gowri@apple.com; Daniel Kurz, Apple Inc., daniel\_kurz@apple.com.

mobile AR is limited camera field of view (FoV) and motion by the user, hence an application is usually able to accumulate less than 90 – 100 degrees effective FoV initially. A virtual object placed in front of the user, however, is expected to reflect what is behind the camera, and parts which are not present in the captured frames. The problem is thus to estimate, given this incomplete environment map, a plausible estimation for the rest of the scene and its lighting.

We show that our method is not only able to correctly estimate the low frequency light information, but also synthesize a high resolution completed scene. For instance in the scene shown in Figure 1(b), the estimated environment map is high resolution, continuous and a plausible extrapolation of the input. The synthesized parts not only match low frequency information (ambient light temperature and intensity), but also finer details such as the type of light sources (in this case, ceiling area lights). As detailed in Section 3, we achieve this context-aware scene completion using the framework of generative adversarial networks (GANs) along with novel loss functions, *ProjectionLoss* and *ClusterLoss*, designed for accurate light estimation.

In popular mobile AR frameworks [ARCore 2020; ARKit 2020], it is possible to obtain camera frames, along with device poses and (low resolution) scene geometry, around the 3D location where the virtual object is to be placed. This allows a real-time rendering engine to create light/reflection probes [UnityTechnologies 2020] at the 3D location, with set extents. RGB texture information from the camera frames can thus be rendered into an equirectangular image at these probe locations. In this work, we focus on processing the partial environment map available at these probes, and thus without loss of generality can handle the spatially varying nature of light in any given AR scene.

We present a method that takes as input a partial environment map that is composed from one or more low dynamic range (LDR) camera frames (8 bit per RGB channel), and outputs a completed environment map that is higher dynamic range (HDR, 16 bit per RGB channel). Thus we perform both lifting of input pixels from LDR to HDR, as well as spatial HDR extrapolation. The output environment map retains the color and details from pixels that were in the input, while filling in the unknown pixels with plausible content that is coherent with the known. That is, we want the completed environment map to represent the textures from a plausible real scene. As shown in Figure 1, and benchmarked in further sections, we demonstrate that our method surpasses the current state-of-the art to estimate high quality, perceptually plausible, and accurate HDR environment maps. We reduce the directional error for lights by more than half, and achieve a significantly lower Frechet Inception Distance (FID) on the generated images.

Related works estimate a subset of the environment map properties, such as lighting direction, color, and intensity using low resolution images [Gardner et al. 2019; Garon et al. 2019; LeGendre et al. 2019], a specific number of parametric lights [Gardner et al. 2019; Hold-Geoffroy et al. 2017], or low dynamic range environment maps [Srinivasan et al. 2020]. Methods that estimate both light and texture [Gardner et al. 2017; LeGendre et al. 2019; Song and Funkhouser 2019] suffer from lack of resolution and detail in the estimated environment map. In contrast, our solution provides sufficient details in the image for virtual objects of any material finish

including reflective mirrors. To create plausible scene completions, we take inspiration from work in the area of generative adversarial networks (GANs) [Goodfellow et al. 2014], which has shown promise in synthesizing realistic images. However, most success for GANs has come for datasets with single objects (e.g. faces [Karras et al. 2018]), using conditional labels [Odena et al. 2017], or self-supervision [Chen et al. 2018]. Its direct use for panoramic images of indoor scenes, small datasets with high appearance variation, and ambiguity in semantic labeling, is challenging. We present *ClusterLoss*, a novel training loss for the discriminator, that allows us to create realistic images with a dataset of only ~2,800 training images.

We also observe that each of the previous methods have a different evaluation scheme, based on respective representations and/or involve subjective user studies. Though subjective plausibility is important for user experience, it makes benchmarking difficult. We present metrics that can be used to quantitatively compare both the lighting and reflection quality of environment maps.

In summary, we make the following core contributions:

- We present a method that can generate an HDR environment map, which is suitable for both reflections (mirror finish materials) and lighting, from a small FoV LDR image or partial environment map. To the best of our knowledge, ours is the first to achieve this for real-time AR applications.
- We present two novel contributions to the training pipeline in the form of *ProjectionLoss* for the environment map, and *ClusterLoss* in the adversarial training process. This allows us to reduce the directional error by more than 50% compared to current methods, while achieving 3.7 times lower FID.
- We establish metrics that allow fair and quantitative comparisons with related work, and thus provide a systematic benchmark for this emerging area in AR.
- Our contributions allow training of efficient network architectures, which we use in our real-time demo mobile app that takes less than 9 ms per inference on an iPhone XS.

## 2 RELATED WORK

The classical technique to obtain an HDR environment map is to merge images of a mirror sphere in the scene captured under multiple exposure brackets [Debevec 1998]. This can be applied for offline use cases, such as games and artistic renderings, but is unsuitable for real-time mobile AR applications in arbitrary and previously unseen environments. Early work on environment map estimation used scene geometry and/or ground plane estimation to warp the small FoV image into an equirectangular image [Lalonde and Efros 2010]. Several techniques using image mirroring, special handling for sky pixels, and texture synthesis were proposed for creating the reflection maps, but there was no single end-to-end solution for general and real-time use. The problem of light estimation was not addressed in this work, but dynamic range extrapolation was performed by reversing the camera response function and arbitrarily increasing radiance of saturated pixels.

There have been many previous works on light estimation from images using additional cues about an object [Marschner and Greenberg 1997], scene geometry [Azinović et al. 2019; Maier et al. 2017; Zhang et al. 2016], or special cases such as outdoor sun position

estimation [Hold-Geoffroy et al. 2019, 2017; Zhang et al. 2019]. For brevity, we only discuss works that focus on light estimation from small FoV images of general scenes. In this context, we find works broadly divided into two categories: those that focus on light estimation with low dimensional parametric forms, and those which estimate both lighting and environment maps.

Garon et al. [2019] use spherical harmonics representation for light and depth estimated using the SUNCG dataset [Song et al. 2017]<sup>1</sup>. Cheng et al. [2018] also predict 48 spherical harmonics coefficients as lighting from two images captured by the front and rear cameras of a mobile device. Gardner et al. use parametric lights as representation [2019]. The parameters are derived using peak finding and region growing on intensity images, followed by fitting of ellipses. Even though use of parametric lights reduces the size of their network decoder, the authors use a loss function that is derived by converting the parameters to an equirectangular image followed by L2 loss. It is not clear how to extend this method to generate higher quality texture in the environment map images that would be consistent with the regressed low dimensional parameters. We thus choose to have an end-to-end network that directly estimates the HDR environment map. However, the extraction of parametric lights from an environment map proposed by Gardner et al. [2019] is a useful representation for analytical lights, and we use it to create quantitative metrics for benchmarking (See Section 4).

Gardner et al. use equirectangular RGB and intensity maps as representation [2017]. They divide the task into light position estimation (using LDR panoramic images), and HDR intensity estimation (using the Laval HDR Images dataset). This is the work most similar to our method in input-output, representation, and formulation. In contrast to their method, we have a single stage training from an LDR small FoV image to a completed HDR environment map, and using our proposed adversarial training we are able to generate more realistic RGB scene completion for use on reflective virtual objects. Some recent works, similar to our method, employ adversarial loss to generate a completed environment map image [Song and Funkhouser 2019; Srinivasan et al. 2020] or sphere images [LeGendre et al. 2019]. LeGendre et al. captured a special dataset with three spheres of mirror, matte, and diffuse gray finish [2019]. They train a neural network to regress from a camera image to three small ( $32 \times 32$  pixel) images representing the sphere segments. This again limits use of the results for rendering high quality reflections. Even more importantly, due to the low resolution, the estimate covers mostly the portion of the scene behind the camera. It is useful to render a given frame, but if the camera were to move with respect to the virtual object then a new estimate has to be inferred from the trained model. Thus even with the assumption of a static scene and only camera motion, their method would suffer from temporal flickering due to multiple independent estimates as the user moves around the virtual object.

Song et al. employ a multi-stage ensemble that estimates geometry, LDR completion and HDR illumination [2019]. Our method uses a single model compared to their large multi-stage ensemble, and we do not require depth-map per HDR image for training. This makes our method efficient to train and use in real-time mobile AR.

<sup>1</sup>SUNCG is currently withdrawn from distribution

The authors do not specify the resolution of the panoramic images, but visual observation shows lack of resolution and artifacts due to the projection from noisy 3D reconstructions. Srinivasan et al. use a stereo pair as input to generate the output environment map [2020]. They use the LDR images from the synthetically generated InteriorNet dataset [Li et al. 2018], to train the light estimation, by application of inverse gamma on the tone mapped images. This limits the ability of the model to learn realistic high dynamic range and accurate lighting, as also indicated by their results on mostly reflective objects. In contrast, our method does not require stereo input, and estimates a high dynamic range environment map that can be applied for lighting objects with wide range of materials from diffuse to mirror.

Furthermore, we employ only 2,100 HDR images of the publicly available Laval HDR Images dataset of real environments, a much smaller dataset than the 4.06 million non-public specialized sphere images used in [LeGendre et al. 2019], the withdrawn SUNCG dataset used in [Song et al. 2017], or the 200,000+ Matterport images in [Song and Funkhouser 2019]. The lack of shared code, model weights and use of private datasets make it difficult to make detailed quantitative comparisons to these recent methods, that also compare to [Gardner et al. 2017] as we do in our quantitative evaluations. However, we present qualitative comparisons to these works in Section 5.

With the exception of the method from LeGendre et al. [2019], that outputs a  $32 \times 32$  sphere image, no other previous method discussed above, has been demonstrated on current mobile devices (smartphones and tablets). To the best of our knowledge, we are the first to demonstrate real-time on-device generation of environment maps of high resolution and high image quality.

### 3 PROPOSED METHOD

As discussed in the introduction, creating a light probe in a mobile AR application involves two broad stages: firstly to select a 3D point as center of this probe and project known scene information to an equirectangular environment map with the selected point as camera center; and secondly to process the partial equirectangular to output a completed HDR environment map. The first requires color (RGB from camera frames) and scene geometry knowledge or assumption for projection. In our work, we assume without loss of generality that platform and application-dependent processing can be used to perform this projection, and obtain the incomplete environment map from the probe center. Using the mobile device pose also helps to ensure that the environment maps are upright or gravity aligned, that is, the floor always appears at the bottom and the ceiling on top. Our focus in this paper is on completion, and LDR to HDR lifting of this incomplete environment map. An overview of our proposed method is shown in Figure 2.

We use the equirectangular representation (height and width of  $128 \times 256$  pixels respectively) for the environment map and create a four channel input (RGB-mask). Known RGB pixel intensities are normalized to  $[-1.0, 1.0]$ , while the unknown pixel are populated with random noise from a uniform distribution  $U(-1.0, 1.0)$ . The fourth channel is a binary mask with known pixels marked with 0 and unknown with value 1. This is input into our network,

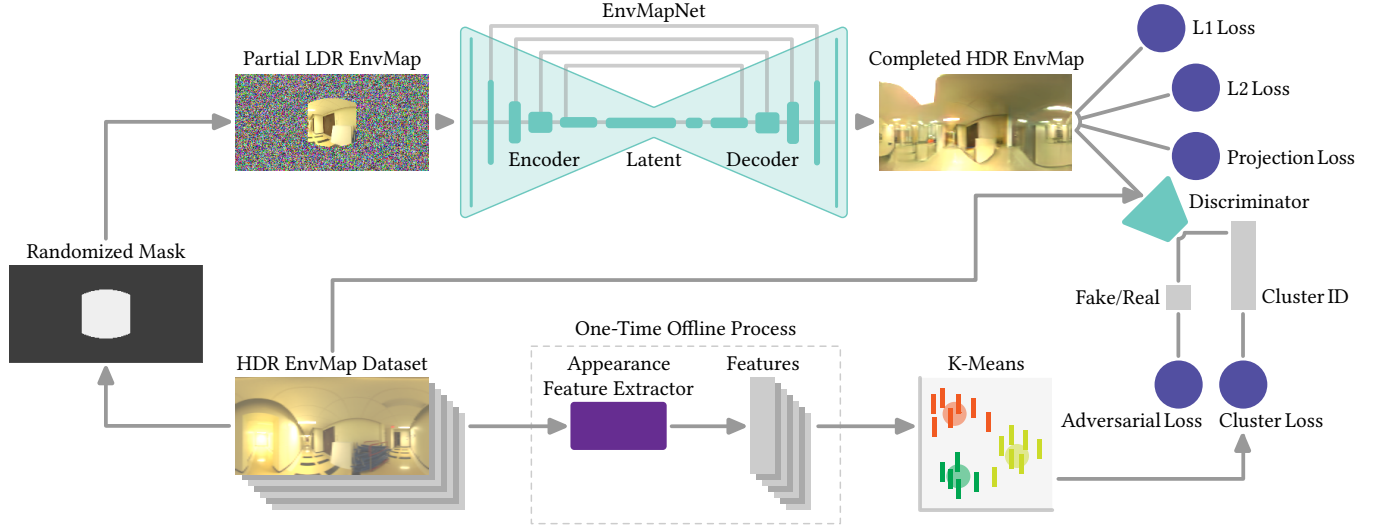


Fig. 2. Overview of our method: We propose EnvMapNet, an encoder-decoder network with skip connections, that outputs completed HDR environment maps from partial input. We train the network end-to-end in an adversarial setup. An offline one-time clustering of the training images is used to provide a supervised classification task for our novel ClusterLoss in the discriminator. The additional adversarial loss, along with our proposed ProjectionLoss, allows our method to generate high quality environment maps for reflection and accurate shading of virtual objects.

EnvMapNet, that outputs a three channel, HDR RGB image in log scale (detailed in Section 3.1). The log scale image is converted to linear values, optionally decomposed into analytical light sources, and provided to the rendering engine on the platform. We train our network end-to-end with a combination of image-based and adversarial losses (Sections 3.3 and 3.4), which allows us to handle both the generative aspect for reflection map completion and light estimation from partial environment map. We detail the different aspects of our pipeline in the following subsections.

### 3.1 Dataset and Processing

In this work we employ two publicly available datasets: Laval Indoor HDR dataset [Gardner et al. 2017], and PanoContext LDR panoramas [Zhang et al. 2014]. We use the same test split for the Laval dataset as Gardner et al. [2017]<sup>2</sup>, and the remaining 2,810 images for training. The range of intensities from different sources and scenes varies largely and is unsuitable for stable training as-is, hence we employ a log scale on exposure-normalized HDR linear images for training the network. The LDR images from PanoContext are useful to train for reflection and the discriminator. For a given linear HDR ground truth image  $G_{lin}$ , we compute the training ground truth  $G$  as follows:

$$G = \min(\max(0, \log_{10}(G_{lin} \cdot \alpha + 1)), 2) - 1, \quad (1)$$

We empirically choose  $\alpha = 0.2 \cdot \overline{G_{lin}}$  to match the middle gray values. The clipping of intensities corresponds to our use of tanh activation for our network, and results in dynamic range of  $[0, 100]$  for output linear RGB, given the input LDR images in  $[0, 1]$  range.

<sup>2</sup><http://vision.gel.ulaval.ca/jflalonde/projects/deepIndoorLight/test.txt>

### 3.2 Model Architecture

Our proposed model, EnvMapNet, consists of an encoder and decoder as shown in Figure 2. Each is composed of several building blocks detailed in Table 1 for reproducibility. The encoder is composed of five sets of EnvMapNet-conv-block and EnvMapNet-downsample-block, with  $uk=[64, 128, 128, 128, 256, 256, 512]$  for each consecutive block respectively. The resulting latent vector is convolved with a  $1 \times 1$  kernel to output 64 filters. The decoder mirrors the encoder by using EnvMapNet-conv-block and EnvMapNet-upsample-block. The final output is produced by a  $3 \times 3$  convolution to produce 3 channels for RGB, followed by a tanh activation. We use skip connections between layers of the encoder and decoder with same dimensions, as depicted in Figure 2. Spectral Normalization [Miyato et al. 2018] is used in all convolution layers of EnvMapNet and the discriminator for stable training.

### 3.3 Image-based Regression Losses and ProjectionLoss

We use a weighted combination of image-based regression and adversarial losses to train our model end-to-end. For the image-based losses, we want to retain the color and details for pixels from the known (input) region while hallucinating the rest with a plausible, perceptually pleasing scene completion (typically extrapolation). Guided by the binary mask in the input, we compute an  $L1$  loss between the known pixels in the input and the predicted RGB values in the same locations. For the completed output, we apply a multi-scale  $L2$  loss implemented with pooling layers for efficient training. This allows the model to coarsely regress the light direction and color, however it does not allow for generation of sharp features for the estimated light sources (as seen in Figures 1 (b) and 2). To obtain a high contrast HDR result that generates correct shadows, the network needs to be penalized for both generating high intensities

(a) ProjectionLoss	0.37	0.25	0.35	3.13	0.63	0.43	
(b) AngularError	21.4	22.9	24.2	103.9	107.2	109.86	
(c)							
(d)							
	Reference	Example 1	Example 2	Example 3	Example 4	Example 5	Example 6

Fig. 3. Representative results for metrics and losses correlated to directional error of estimated lights. Row (a): Our proposed projection loss on the environment maps w.r.t Reference (see Section 3.3). Row (b): The angular errors in degrees, using parametric lights for each environment map w.r.t Reference (see Section 4). Row (c): Environment maps with extracted parametric lights shown as red ellipses. Row (d): Rendering of a rough metallic sphere using the corresponding environment map and viewed from top. All environment maps used are ground truth images from the Laval Indoor HDR Images dataset.

<b>EnvMapNet-conv-block</b>
short-cut,x=input
Repeat 5 times:
x=BatchNormalization(x)
x=LeakyReLU(slope=0.2)(x)
x=Convolution(kernel=(3,3),filters=16)(x)
x=Concatenate(x,short-cut)
short-cut=x
output=x
<b>EnvMapNet-upsample-block</b>
x=input
x=NearestNeighbourUpsample2x(x)
x=Convolution(kernel=(3,3),filters=uk)(x)
output=x
<b>EnvMapNet-downsample-block</b>
x=input
x=Convolution(kernel=(3,3),filters=dk)(x)
x=AveragePool2D(x)
output=x
<b>Discriminator-residual-block</b>
sc=AveragePool2D(input)
sc=Convolution(kernel=(3,3),filters=ak)(sc)
x=input
Repeat 2 times:
x=BatchNormalization(x)
x=LeakyReLU(slope=0.2)(x)
x=Convolution(kernel=(3,3),filters=ak)(x)
output=Add(x,sc)

Table 1. Blocks used in EnvMapNet and the discriminator network.

in the wrong pixels and lack of lower intensities where necessary, which the  $L_2$  loss does not handle well.

An ideal solution would be to use a ray tracer to render shadows and penalize the difference between the images using ground truth and predicted environment map. This however is non-trivial for end-to-end training due to limitations in differentiable rendering

and increase in training time. Considering only shadow casting, the intensity of a pixel in the shadow is dependent on the integral of the environment map except for directions blocked by the object. Thus, any pixel on the shadow plane can be approximated by the integral over the masked environment map. We take inspiration from our intuition above, and Wasserstein (Earth Movers) distance, and introduce our novel ProjectionLoss. We select a set of random binary masks  $P$  having the same size as our environment map, and create a one-dimensional vector of length  $|P|$  by integrating the pixel intensities in corresponding masked images. On a 0-valued background, the masks contain randomly generated polygons with a value of 1, whose height and width range from 10% to 40% of the corresponding image dimensions. We show some examples of the masks in Appendix A.1. The final loss, termed ProjectionLoss, is the  $L_1$  distance between the vectors corresponding to predicted and ground truth environment maps. We show this error using  $|P| = 50$  projection masks in Figure 3 (a) for each environment map shown in row (c), with the first image being the reference. In Figure 3 (d) we show rendered spheres using the corresponding environment maps. We can see that lower values of ProjectionLoss correlate with both lower angular error, and better visual match of lighting direction to the reference.

The final image-based loss is defined as follows. For a ground truth LDR image (from PanoContext dataset) we only apply the masked  $L_1$  loss and an adversarial loss as discussed next. For a ground truth HDR image  $G$ , a mask indicating unknown pixels  $M$ , a predicted image  $I$ , and a set of projection masks  $P$ , we compute  $Loss_{image}$  as follows.

$$\begin{aligned}
 Loss_{projection} &= |\forall_{P_i \in P} (\sum (I * P_i) - \sum (G * P_i))|_1 \\
 Loss_{image} &= w_1 |I * M - G * M|_1 \\
 &\quad + w_2 ||I - G||_2 \\
 &\quad + Loss_{projection}
 \end{aligned} \tag{2}$$

To further understand the value of ProjectionLoss for lighting estimation, and to compare to other measures, such as SSIM [Zhou Wang et al. 2004] and Mean Squared Error (MSE), we performed the

Metric	Reference Image	Top-5 Retrievals				
(a) SSIM						
(b) ProjectionLoss						
(c) MSE						

Fig. 4. Retrieval for two reference images based on (a) SSIM on rendered images, (b) ProjectionLoss and (c) MSE on equirectangular images. User study on 380 reference images showed 95% agreement with SSIM retrieval. Average intersection with top-5 retrieval from ProjectionLoss was 1.6, and from MSE was 0.6. See Section 3.3 for details.

following experiments. For each dataset environment map, we render an image of a scene with multiple geometric objects as shown in Figure 4. We propose using the SSIM score, which is a metric often used to measure human perception and image similarity, to quantify the similarity of our rendered images. To validate this for our application, we perform a user study asking participants to choose from four provided options which rendered image looks most similar to a reference rendered image. The four options were randomly selected such that two of them were in the top-10 as retrieved by SSIM, and the other two from outside the top-10. Based on the results of 5 study participants, each providing their selection for 380 reference images, we found that on average human participants selected one of the top-10 SSIM images 95% of the time. Hence retrieval of similar environment maps based on SSIM between rendered images is a baseline method to find environment maps that produce similar lighting on the objects.

We then evaluate the correlation between SSIM on rendered images, with ProjectionLoss and MSE calculated on the corresponding (equirectangular) environment maps. We can observe that the retrieval of similar environment maps by ProjectionLoss is better matched with retrieval based on SSIM compared to using MSE, see Figure 4. Quantitatively, we found the intersection of top-5 retrievals by SSIM (on the rendered images) and those using ProjectionLoss (on the environment map) to be  $1.6 \pm 0.7$ , while it was  $0.6 \pm 0.5$  using MSE (on the environment map).

Based on the above we believe that our proposed ProjectionLoss is a good loss to train the network for estimating lighting such that the end result for rendering is accurate with respect to ground truth. Secondly, we show that MSE on the environment map is insufficient for training accurate light estimation, and its use as a metric of comparison or benchmarking, as done in previous works, would not correlate well with the final application.

### 3.4 Adversarial Loss and ClusterLoss

To generate perceptually pleasing and detailed completions to the scene we train the model using a GAN loss. The idea of adversarial training was proposed in [Goodfellow et al. 2014], where a second network (discriminator) was trained to classify samples from the training set as “real” and those produced by a generator as “fake”. The generator is trained with a loss to “fool the discriminator”, or in practice classify generated samples as “real”. The two adversary networks are trained by alternating the update of their weights, usually after every mini-batch. Since their advent, there have been various improvements on GANs focussed on aspects of training stability and result quality. As discussed previously, many of these have focused on single salient objects such as faces [Karras et al. 2018] or increased stability from use of extremely large datasets and/or architectures [Brock et al. 2019]. However, we found that training a mobile-friendly GAN architecture with fewer than 3,000 images with high variability in content was unstable. That is, for various choices of hyper-parameters the generator would face mode collapse (produce very similar images for different inputs), or not converge to visually appealing images.

We know from previous work on GANs that providing an additional task to the discriminator through conditional labels or self-supervision can increase stability [Odena et al. 2017]. Assigning semantic labels, such as room types, is however non-trivial for panoramic images since the camera viewpoint could be from between two rooms. Given that most Laval Indoor HDR images are of public spaces (large warehouses, libraries, hallways), and those in PanoContext are mostly residential rooms, the distribution on any semantic label would be hard to balance. Recent work using self-supervision with rotation prediction as an additional task for the discriminator [Chen et al. 2018] has been promising. However, for equirectangular images the only possible rotations would be flips along the two image axis, of which, that along the vertical image axis is valid for a scene.

We thus propose a novel scheme combining the learnings from above methods, to train on our modest dataset and application. We begin with the recognition that our application needs to generate “plausibly similar looking images” as the training set, hence the idea to use appearance features to form a secondary supervision task. We use traditional image-based features (the mean color and ORB descriptor [Rublee et al. 2011] for image patches) and assign a K-means-derived cluster ID to each image (we empirically selected  $K = 5$  clusters). This is computationally efficient during training and adds no cost to the inference, which is critical for real-time mobile AR applications. Along with the typical real vs. fake classification, the discriminator is supervised to classify the K-means assigned cluster ID for each real image with the proposed ClusterLoss. This allows us to train without additional heuristics or tricks, and avoid mode collapse, as the encoded latents are forced to spread out over the appearance clusters. Intuitively it also helps the discriminator focus on a low ambiguity appearance-based task that pays attention to spatial locations and details, thus avoiding cases where early on in the training process a single patch artifact can easily clue the discriminator that the image is fake (that is, avoid “easy wins”). The discriminator is composed of residual blocks as detailed in Table 1,

with  $ak = [64, 128, 256, 256, 256, 256, 256]$  for consecutive blocks respectively. The final outputs for the classifications of real/fake and K-means cluster ID is obtained by convolution of the corresponding output channels and global average pooling. Similar to EnvMapNet, we use Spectral Normalization [Miyato et al. 2018] for all convolution blocks in the discriminator. We use softmax cross entropy loss for the adversarial training of our model and discriminator,  $D$ . With  $y, p$  indicating the ground truth and predicted one-hot encoded vectors for the cluster classification respectively, our adversarial training losses are:

$$\begin{aligned} Loss_{cluster} &= \sum_{k=1}^5 y_{o,k} \log(p_{o,k}) \\ Loss_{fakereal} &= \log(D(G)) + \log(1 - D(I)) \\ Loss_{adversarial} &= -\log(D(I)) \end{aligned} \quad (3)$$

### 3.5 Implementation and Adversarial Training

During training, we mask the ground truth images using randomly generated polygonal regions, and provide them as corresponding incomplete input environment map. The regions are of irregular shape and can be non-contiguous to generalize our model to complete any partial input. Since the Laval Indoor HDR training images have missing information in the lower region (where the tripod was presumably located during capture), we use several augmentation techniques during training. We randomly select one of the following image processing steps: crop the image to exclude the bottom region and resize the crop to the correct aspect ratio, mirror the pixels from above the missing area, or repeat the last fully known row. For input, we tonemap the ground truth HDR environment map by dividing the pixels by the average intensity (exposure compensation), applying a gamma transform with a value of 2.2, and performing a normalization and clipping of the intensity range to  $[-1.0, 1.0]$ . We use the logarithmic transform detailed in Section 3.1 for the ground truth used in evaluation of network losses. The components of  $Loss_{image}$  are weighted using  $w_1 = 0.5$ ,  $w_2 = 0.01$ . For all image-based losses, we also weigh the image pixels to compensate for the subtended angle on the sphere.

We train the networks end-to-end by minimizing  $Loss_{EnvMapNet}$  and  $Loss_{discriminator}$  for EnvMapNet and the discriminator respectively. We use the Adam optimizer, a batch size of 16, and the learning rate starting at 0.0002, and decayed by half every 50 epochs after the first 100 epochs. We alternate between training the discriminator and EnvMapNet after each mini-batch.

$$\begin{aligned} Loss_{EnvMapNet} &= Loss_{image} + Loss_{adversarial} + Loss_{cluster} \\ Loss_{discriminator} &= Loss_{fakereal} + Loss_{cluster} \end{aligned} \quad (4)$$

## 4 METRICS FOR BENCHMARKING

Visual coherence in mobile AR aims to give a user the illusion that an inserted virtual object belongs in the real scene. However development of algorithms, especially in the domain of deep learning, involves many heuristics, hyper-parameter tuning, and experimentation. We therefore believe that establishing quantitative and repeatable metrics, separate from selected loss functions, that closely



Fig. 5. Representative results for parametric lights (shown as red outlines of ellipses) extracted from panoramas. (See Section 4).

correlate with the target application setting, is important both for individual researchers and the community as a whole, to compare different methods. Several previous methods have used MSE on environment maps in RGB, intensity or log formulation as a metric. However, as demonstrated in Section 3.3, it is not well suited to measure accuracy such that the final rendering matches ground truth. Thus we explore and propose the following.

At the core of it we want to solve for two aspects of the IBL: perceptual plausibility and lighting accuracy. In the context of real-time mobile rendering, analytical lights (point lights) are used to render shadows. Hence lighting accuracy for mobile AR is correlated to directional accuracy of top-n dominant light sources, and correctness of cast shadows. Since we cannot (and should not) generate the exact unseen test room for reflection, measures such as MSE or SSIM [Wang et al. 2003; Zhou Wang et al. 2004] for one-to-one image comparisons are unsuitable. Instead we need to use plausibility of the hallucinated scene as a metric. We start with a discussion on lighting accuracy metrics followed by quantitative measures for perceptual quality. Our goal is to define and provide metrics that can be used by any future work to objectively compare techniques. Thus we establish a quantitative and repeatable benchmark that employs the publicly available Laval Indoor HDR dataset [Gardner et al. 2017], and reference implementations of the metrics that we will provide.

Several methods can be used to extract light sources from environment maps, such as median cut [Debevec 2006], variance minimization [Viriyothai and Debevec 2009], and parametric fitting from peak finding as recently proposed in [Gardner et al. 2019]. In the case of mobile AR, real-time rendering engines are likely to employ simple and fast decomposition techniques, hence we use the latter method to find centers and extent of light sources in an IBL. The angular/spherical coordinates of the center (of the ellipse) is used to measure the directional accuracy with respect to ground truth (lower is better). For a given HDR environment map, we recursively find a seed pixel with maximum intensity, and grow the region connected to the seed till we reach 30% of the peak value. This is repeated until the peak value found is less than 90% of the largest. For each such region, we fit an ellipse covering its convex hull.

Examples of images with parametric light fitting are shown in Figure 5. To measure the final AngularError between the ground

truth and estimated environment maps, we first extract (at most) five parametric lights from each. For each ground truth light from an environment map, we find the minimal angular error to the predicted light set, and vice-versa, for each predicted parametric light we find the least angular error to a ground truth light. We take the mean over the errors from both ground truth lights and predicted lights, as the final AngularError between the two environment maps. Figure 3 demonstrates the correlation of the angular error metric, with examples of low and high errors with respect to a selected reference IBL. We used Tungsten<sup>3</sup> to render a sphere with “roughconductor” material (Al), albedo and roughness of 0.5. We can see that environment maps with lower errors produce similar lighting directions on the reference sphere, compared to those with higher errors, thus making it a suitable metric for comparison.

To measure perceptual plausibility, user studies are commonly employed for their insight into final user experience quality. However, user studies are hard to repeat or compare across different publications. We take inspiration from work in GANs, that measure quality of synthesized images using Frechet Inception Distance (FID) [Heusel et al. 2017]. The measure is defined to evaluate similarity of distributions between two image sets, in contrast to perceptual metrics such as SSIM that require a reference image for each given test image. That is, the FID is low between two sets of images that have similar image features, and overall diversity among the different generated samples is the same as in the reference samples. This metric is thus good to demonstrate that not only do the details in any generated environment map match realistic patches from training images, but the set of predicted IBLs also have variety in content, without over-fitting to any one (or select few) training scene. For each equirectangular image, we extract several crops of different FoV. We resize each crop to 299×299 pixels and obtain the feature from an Inception-v2 network, pre-trained on ImageNet<sup>4</sup>. For comparisons in Section 5 we calculate the FID on feature sets obtained from the training images and predicted results, from different methods, on the test set.

## 5 RESULTS

In this section we provide several results to demonstrate the effectiveness of our method for rendering virtual objects in mobile AR applications. We start with qualitative, real-world application of our model, followed by quantitative comparisons and benchmarking results. All images are best seen on a digital color monitor.

### 5.1 Qualitative Results

In Figure 6 we show results from our prototype iOS app used in real-world scenes. We use device pose and plane geometry provided by ARKit [ARKit 2020] to warp the input camera image into a partial environment map. The completed environment map from running our model on the device is then used with SceneKit<sup>5</sup> to render the virtual object<sup>6</sup>. The inference time is under 9 ms on an iPhone XS. Please see the **supplementary material** for videos from our real-time mobile application. We have also provided higher resolution

<sup>3</sup><https://github.com/tunabrain/tungsten>

<sup>4</sup><https://keras.io/applications/#inceptionresnetv2>

<sup>5</sup><https://developer.apple.com/documentation/scenekit/>

<sup>6</sup>3D models from <https://developer.apple.com/augmented-reality/quick-look/>

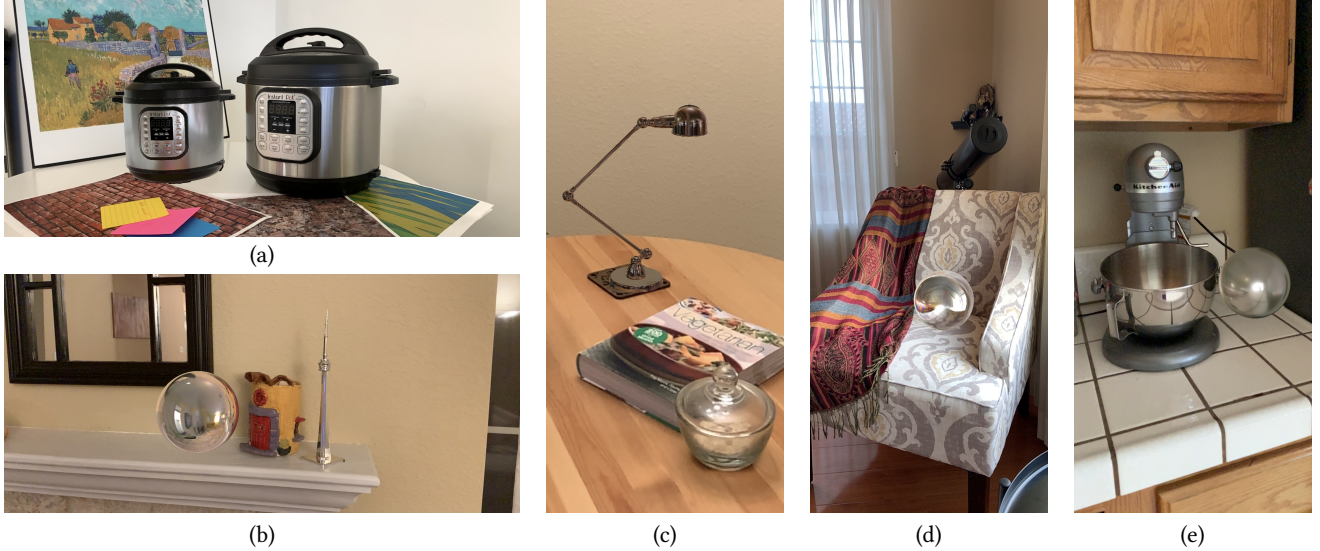


Fig. 6. Snapshots from our real-time prototype application. (a) We show a real and virtual rendering of same object, we can see that the lighting direction and color matches closely. Note that the materials on virtual do not exactly match the real (anisotropic roughness on the steel body). (b) A mirror finish metallic sphere is rendered in a scene, we can see the lighting direction is coherent with other real objects in the scene and the reflection formed is also a plausible completion to the scene. (c) A virtual lamp is placed on the table, and its top specular highlight matches the direction also seen on the glass object on the lower right. (d)-(e) We render metallic spheres with different roughness with other objects in the scene for reference. All images are best seen in color. Please see the **supplementary material** for videos from our real-time app and Appendix A.2 for higher resolution.

crobs from the images in Appendix A.2 for better observation. Figure 6(a) shows a real cooker in the right, and a rendered version on the left (please note, that the exact material properties of the steel body do not match). We can clearly see that the lighting direction closely matches the reference real-world object, providing the correct specular highlights on the object. The accurate lighting, combined with perceptually plausible reflection clearly makes the rendering an immersive AR experience. In Figure 6(b) we render a mirror sphere into a scene to show the impact of generating plausible reflections. Though the input observes a very small part of the environment, we are able to create a believable AR experience by completing the environment map with a detailed scene. Even though it cannot match the actual room in every detail, the perceptual impact and coherence of the virtual object with other objects, such as the mirror on the wall, and metallic tower on the right, is evident. In Figures 6(c)-(e) we provide more examples of inserted virtual objects that have coherent lighting with the other objects in the field of view.

From the images in Figures 1 and 6 we highlight a few aspects of our method. For each of the scene types, that vary in time of day and FoV, not only is the light direction coherent with the scene but so is the type/shape/size of light source generated by our method. For instance, Figure 1(e) shows a virtual teapot on a table illuminated with an unseen artificial light. The roughness of the teapot was set to 0.2, with 1.0 metalness in SceneKit. The light direction and highlights from our estimate closely match those observed on the real teapot (blue) and sphere (pool ball) in the scene. In Figures 6(b) and (d) the light sources have appearances closer to that of a window/door that are common and plausible in those environments.

We made qualitative comparisons to recently published work from [Srinivasan et al. 2020] in Figure 12. The authors also provided results from their re-implementations of [Song and Funkhouser 2019] and [LeGendre et al. 2019]. We discuss the results in detail in Appendix A.4.

## 5.2 Quantitative Evaluation and Benchmarking

For quantitative benchmarking we use the metrics detailed in Section 4, and show the results in Figures 7 and 8, and Table 2. As discussed in Section 2, though several methods have focused on light estimation from single images, only a few generate HDR RGB environment maps. Recent techniques that estimate lighting such as [Song and Funkhouser 2019] and [LeGendre et al. 2019], have not shared code, model weights or use common public datasets. There is also a lack of a standard set of metrics for comparison. The method by [Gardner et al. 2017] is the current state-of-the-art method that is most comparable to our method, uses the same public dataset, and is compared in the above recent works as well. They have provided a web interface to obtain results from their method<sup>7</sup>. Since we also use the same splits from the Laval Indoor HDR Images for training/testing, and it is the current state-of-art in HDR environment map estimation, we provide detailed quantitative and qualitative comparisons with their results.

In Figures 7 and 8 we show predicted environment maps from both methods over a variety of scenes and lighting conditions. We further show their use for rendering both reflective (teapot) and

<sup>7</sup><http://rachmaninoff.gel.ulaval.ca:8001/>

Metric	EnvMapNet (Ours)	Ours without ProjectionLoss	Ours without ClusterLoss	Gardner et al. [2017]	Artist IBL (Fixed)
FID	52.7	77.7	203.0	197.4	-
AngularError (mean $\pm$ std)	34.3 $\pm$ 18.5	39.2 $\pm$ 29.9	75.1 $\pm$ 25.0	65.3 $\pm$ 24.5	46.5 $\pm$ 15.4

Table 2. Quantitative comparison on metrics averaged over 250 test images from Laval HDR dataset. For both metrics lower is better. See Section 4.

diffuse (dragon) objects<sup>8</sup> with shadow. Each result is shown over a pair of rows containing the input crop, rendered images, and corresponding environment maps with angular error below each. To enable fair and future comparison, we crop the test IBLs in the center for 90 degree FoV. We rectify and provide the **Input Crop** to [Gardner et al. 2017], and project them to a equirectangular map for our method. We obtain the predicted equirectangular maps from each image, extract the parametric lights for calculation of AngularError as described in Section 4, and proceed to use for rendering. We use Tungsten, to generate renders for an aluminum metal finish teapot and a lambertian material on the dragon objects. Only for the purpose of rendering, we perform the following post-processing operations on each predicted equirectangular map. Since each method provides the result in an arbitrary intensity range, we scale the pixel intensities for each predicted result such that the average intensity in the region provided as input is equal to that of the ground truth HDR. We further overlay the pixels from the ground truth corresponding to the input FoV, to simulate the AR video backdrop and common background for each rendering. We provide this equirectangular map as the input for Tungsten, position the virtual camera to match the input crop provided, and obtain the rendered images shown in Figures 7 and 8 for **EnvMapNet (Ours)**, **Ground Truth** and **[Gardner et al. 2017]**. We stress that this post-processing was only done for the offline rendering pipeline and not for other comparisons.

As previously detailed, this simulates that a virtual object is placed at the center of a probe which is illuminated using the IBL. As shown in the images, our results generate perceptually pleasing and accurate lighting for the virtual object compared to those from [Gardner et al. 2017], for both material finishes. Though our method cannot (and should not) create the unseen ground truth scene exactly, the level of detail generated is clearly plausible and provides a better visual coherence compared to those from [Gardner et al. 2017]. This aspect regarding image resolution and quality of the details is captured by the FID metric. The renderings of the diffuse dragon object on a plane, highlight the difference in accuracy of estimated light direction, as captured by our AngularError metric listed below each result. The images show estimated environment maps with a wide range of errors from both methods, and as can be observed, overall our estimates produce shadows which better match those from the ground truth IBL.

We provide the quantitative metrics in Table 2, calculated over the 250 test images from the Laval Indoor HDR Image dataset. The results from using our complete method are reported as **EnvMapNet**. We introduced two novel loss functions in our method, for which we also conducted ablation studies. **Ours without ProjectionLoss**,

corresponds to our model trained with all loss functions except the proposed ProjectionLoss. We observe that the angular error is higher than our full model EnvMapNet, as expected from our discussions in Section 3.3. When we trained **Ours without ClusterLoss**, for the discriminator, the model often suffered from instability as discussed in Section 3.4, and could not generate textures with fine details, hence the higher FID and angular error. The errors for **[Gardner et al. 2017]** are higher than our complete pipeline. As shown with examples, the environment map generated by their method lacks fine details for the scenes hence the higher FID score. The angular error is also higher on average, which could be explained from our experiments in Section 3.3 that show MSE loss is insufficient to train for accurate lighting. As a baseline measurement, we consider that applications may use a fixed/default environment map, created by an artist, for lighting. We obtained such an environment map created for indoor scenes as detailed in Appendix A.3. We calculate the angular error metric with respect to this artist designed IBL, and report it as a baseline for our benchmarking in Table 2 as **Artist IBL**. As demonstrated through the examples and benchmarking, our method, with lowest FID and AngularError, can produce high quality environment maps both for visually pleasing reflections, and accurate lighting of the virtual objects.

## 6 LIMITATIONS

Our method provides a perceptually plausible completion to the partial environment map using the equirectangular representation. It is an efficient representation for 2D convolution operations but has two disadvantages: the vertical seam from sharp color change between the first and last column of the image, and the disproportionate number of pixels used for the top section (commonly texture-less in indoor scenes). We could reduce visibility of the seam using a blending operation or rotating the environment map where possible, such that the edge appears away from the current user viewpoint. A future direction is finding a more general solution, such as a loss function that can be incorporated into the end-to-end training. In our current implementation we weigh the image-based losses for the environment maps to compensate for the subtended angle on the sphere, to account for sampling issues on the top and bottom regions. An alternate approach would be using spherical convolutions that were shown as efficient for feature extraction in equirectangular images [Su and Grauman 2017]. Wide-spread application of AR in the real world requires rendering consumer objects that commonly have non-diffuse material finishes. We demonstrated through our results and comparisons that high frequency details are essential for plausible reflections, in our case with  $128 \times 256$  pixel resolution environment maps. We believe that this is just a starting point, and further research with images of general indoor scenes

<sup>8</sup><http://graphics.stanford.edu/data/3Dscanrep/>

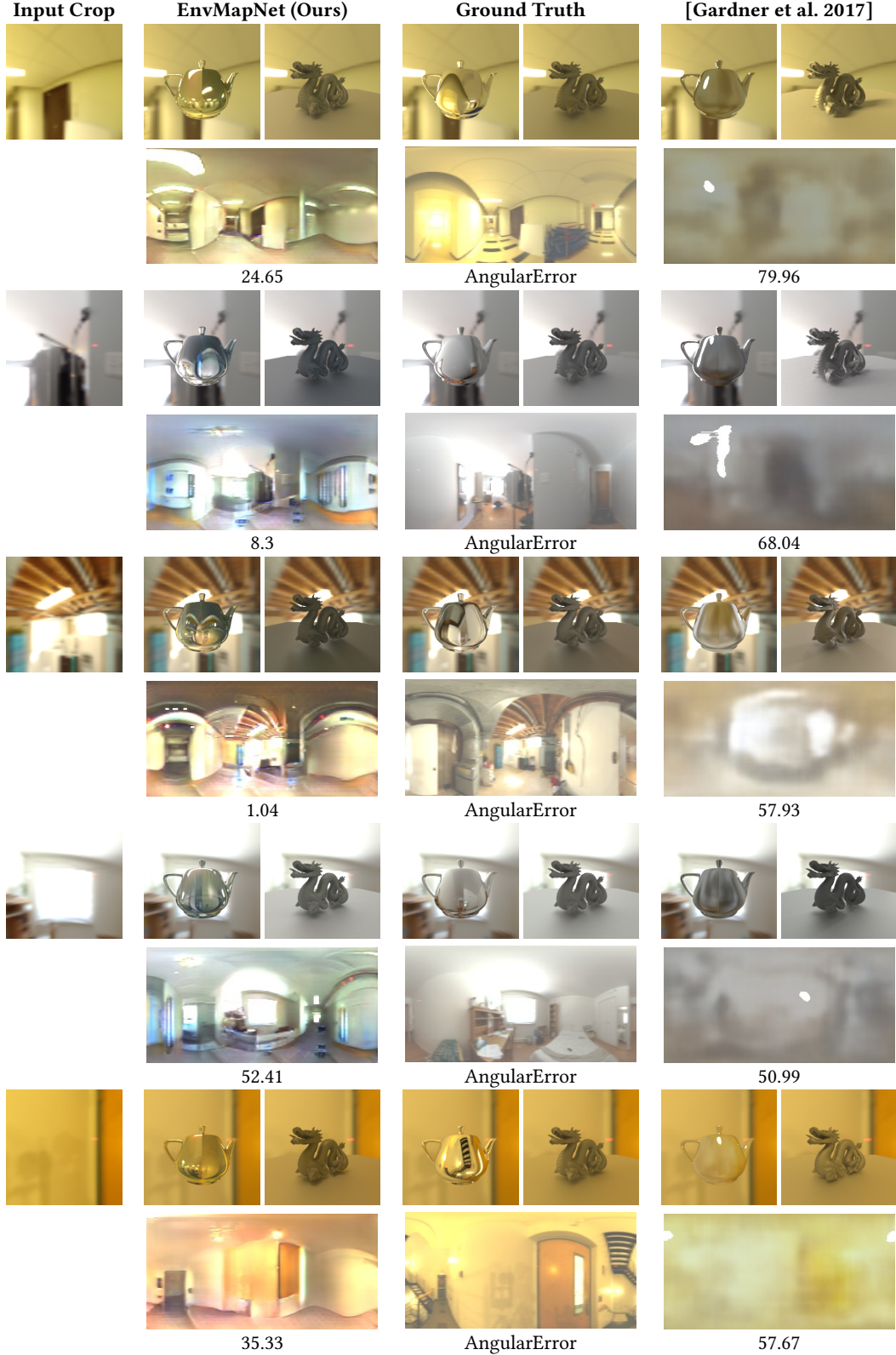


Fig. 7. Results with variety of angular errors. Each result is shown over a pair of rows containing the input crop, rendered images with reflective teapot and diffuse drago, with corresponding environment maps below each. As discussed in Section 5 our method is qualitatively and quantitatively able to produce visually coherent environment maps for both lighting, shadows and reflection.

is essential to reach higher image quality, similar to generative adversarial models on facial images [Karras et al. 2018].

## 7 CONCLUSIONS

In this work we presented the first method that, given a small field-of-view LDR camera image, can estimate a high resolution full HDR environment map in real-time on a mobile device. The result can be used to light objects of any material finish (mirror to diffuse) for augmented reality. We made two novel contributions in the training of our neural network, with *ProjectionLoss* for the environment map, and *ClusterLoss* for the adversarial loss. We showed based on user studies and quantitative measures that *ProjectionLoss* correlates to visual perception of similarity in shading of virtual objects. This enabled our method to synthesize environment maps with accurate lighting and perceptually plausible reflections. We proposed two metrics to measure both these aspects of the estimated environment map. Through qualitative and quantitative comparisons with the current state-of-the-art, we demonstrated that our method reduces the angular error in parametric light direction by more than 50%, along with a 3.7 times reduction in FID. We showcased real-world application using a mobile app, that is able to run our model in real-time (under 9ms), and render visually coherent virtual objects in previously unseen environments.

## REFERENCES

ARCore. 2020. *Google LLC*. <https://developers.google.com/ar>

ARKit. 2020. *Apple Inc*. <https://developer.apple.com/augmented-reality>

Dejan Azinović, Tzu-Mao Li, Anton Kaplanyan, and Matthias Nießner. 2019. Inverse Path Tracing for Joint Material and Lighting Estimation. In *Proc. CVPR*.

Andrew Brock, Jeff Donahue, and Karen Simonyan. 2019. Large Scale GAN Training for High Fidelity Natural Image Synthesis. In *Proc. ICLR*.

Ting Chen, Xiaohua Zhai, Marvin Ritter, Mario Lucic, and Neil Houlsby. 2018. Self-Supervised GANs via Auxiliary Rotation Loss. In *Proc. CVPR*.

Dachuan Cheng, Jian Shi, Yanyun Chen, Xiaoming Deng, and Xiaopeng Zhang. 2018. Learning Scene Illumination by Pairwise Photos from Rear and Front Mobile Cameraeras. *Computer Graphics Forum* 37 (10 2018), 213–221.

Paul Debevec. 1998. Rendering Synthetic Objects into Real Scenes: Bridging Traditional and Image-Based Graphics with Global Illumination and High Dynamic Range Photography. In *Computer Graphics and Interactive Techniques (SIGGRAPH)*. 189–198.

Paul Debevec. 2006. A Median Cut Algorithm for Light Probe Sampling. In *ACM SIGGRAPH Courses*. ACM, Article 6.

Marc-André Gardner, Yannick Hold-Geoffroy, Kalyan Sunkavalli, Christian Gagné, and Jean-François Lalonde. 2019. Deep Parametric Indoor Lighting Estimation. In *Proc. ICCV*.

Marc-André Gardner, Kalyan Sunkavalli, Ersin Yumer, Xiaohui Shen, Emiliano Gambaretto, Christian Gagné, and Jean-François Lalonde. 2017. Learning to Predict Indoor Illumination from a Single Image. *ACM Transactions on Graphics (SIGGRAPH Asia)* 9, 4 (2017).

Mathieu Garon, Kalyan Sunkavalli, Sunil Hadap, Nathan Carr, and Jean-François Lalonde. 2019. Fast Spatially-Varying Indoor Lighting Estimation. In *Proc. CVPR*.

Ian Goodfellow, Jean Pouget-Abadie, Mehdi Mirza, Bing Xu, David Warde-Farley, Sherjil Ozair, Aaron Courville, and Yoshua Bengio. 2014. Generative Adversarial Nets. In *Proc. NIPS*. 2672–2680.

Martin Heusel, Hubert Ramsauer, Thomas Unterthiner, Bernhard Nessler, and Sepp Hochreiter. 2017. GANs Trained by a Two Time-scale Update Rule Converge to a Local Nash Equilibrium. In *Proc. NIPS*. 6629–6640.

Yannick Hold-Geoffroy, Akshaya Athawale, and Jean-François Lalonde. 2019. Deep Sky Modeling for Single Image Outdoor Lighting Estimation. 6920–6928. <https://doi.org/10.1109/CVPR.2019.00709>

Yannick Hold-Geoffroy, Kalyan Sunkavalli, Sunil Hadap, Emiliano Gambaretto, and Jean-François Lalonde. 2017. Deep Outdoor Illumination Estimation. In *Proc. CVPR*.

Tero Karras, Timo Aila, Samuli Laine, and Jaakko Lehtinen. 2018. Progressive Growing of GANs for Improved Quality, Stability, and Variation. In *Proc. ICLR*.

Jean-François Lalonde and Alexei A. Efros. 2010. Synthesizing Environment Maps from a Single Image.

Chloe LeGendre, Wan-Chun Ma, Graham Fyffe, John Flynn, Laurent Charbonnel, Jay Busch, and Paul Debevec. 2019. DeepLight: Learning Illumination for Unconstrained Mobile Mixed Reality. In *ACM Transactions on Graphics*.

Wenbin Li, Sajad Saeedi, John McCormac, Ronald Clark, Dimos Tzoumanikas, Qing Ye, Yuzhong Huang, Rui Tang, and Stefan Leutenegger. 2018. InteriorNet: Mega-scale Multi-sensor Photo-realistic Indoor Scenes Dataset. In *British Machine Vision Conference (BMVC)*.

Robert Maier, Kihwan Kim, Daniel Cremers, Jan Kautz, and Matthias Nießner. 2017. Intrinsic3D: High-Quality 3D Reconstruction by Joint Appearance and Geometry Optimization with Spatially-Varying Lighting. In *Proc. ICCV*.

Steve Marschner and Donald P. Greenberg. 1997. Inverse Lighting for Photography. In *Color Imaging Conference*.

Takeru Miyato, Toshiki Kataoka, Masanori Koyama, and Yuichi Yoshida. 2018. Spectral Normalization for Generative Adversarial Networks. In *Proc. ICLR*.

Augustus Odena, Christopher Olah, and Jonathon Shlens. 2017. Conditional Image Synthesis with Auxiliary Classifier GANs. In *Proc. ICML*, Vol. 70. 2642–2651.

E. Rublee, V. Rabaud, K. Konolige, and G. Bradski. 2011. ORB: An efficient alternative to SIFT or SURF. In *Proc. ICCV*.

Shuran Song and Thomas Funkhouser. 2019. Neural Illumination: Lighting Prediction for Indoor Environments. *Proceedings of 33th IEEE Conference on Computer Vision and Pattern Recognition* (2019).

Shuran Song, Fisher Yu, Andy Zeng, Angel X Chang, Manolis Savva, and Thomas Funkhouser. 2017. Semantic Scene Completion from a Single Depth Image. *Proc. CVPR* (2017).

Pratul P. Srinivasan, Ben Mildenhall, Matthew Tancik, Jonathan T. Barron, Richard Tucker, and Noah Snavely. 2020. Lighthouse: Predicting Lighting Volumes for Spatially-Coherent Illumination. In *CVPR*.

Yu-Chuan Su and Kristen Grauman. 2017. Learning Spherical Convolution for Fast Features from 360°Imagery. In *Proc. NIPS*. 529–539.

UnityTechnologies. 2020. *Reflection probes*. <docs.unity3d.com/Manual/ReflectionProbes.html>

Kuntee Viriyothai and Paul Debevec. 2009. Variance Minimization Light Probe Sampling. In *SIGGRAPH '09: Posters (SIGGRAPH '09)*. ACM, Article 92, 92:1–92:1 pages.

Z. Wang, E. P. Simoncelli, and A. C. Bovik. 2003. Multiscale structural similarity for image quality assessment. In *Asilomar Conference on Signals, Systems Computers, 2003*, Vol. 2.

Edward Zhang, Michael F. Cohen, and Brian Curless. 2016. Emptying, Refurnishing, and Relighting Indoor Spaces. *ACM Transactions on Graphics (Proceedings of SIGGRAPH Asia)* 35, 6 (2016).

Jinsong Zhang, Kalyan Sunkavalli, Yannick Hold-Geoffroy, Sunil Hadap, , Jonathan Eisenmann, and Jean-François Lalonde. 2019. All-Weather Deep Outdoor Lighting Estimation. In *IEEE International Conference on Computer Vision and Pattern Recognition*.

Yinda Zhang, Shuran Song, Ping Tan, and Jianxiong Xiao. 2014. PanoContext: A Whole-Room 3D Context Model for Panoramic Scene Understanding. In *Proc. ECCV*.

Zhou Wang, A. C. Bovik, H. R. Sheikh, and E. P. Simoncelli. 2004. Image quality assessment: from error visibility to structural similarity. *IEEE Transactions on Image Processing* 13, 4 (2004).



Fig. 8. More results with variety of angular errors. Each result is shown over a pair of rows containing the input crop, rendered images with reflective teapot and diffuse drago, with corresponding environment maps below each. See Figure 7 and Section 5.

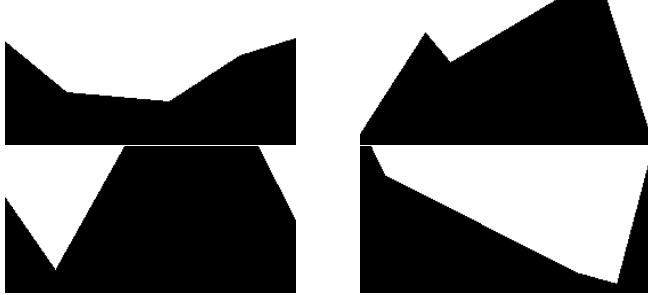


Fig. 9. Example masks used for ProjectionLoss defined in Section 3.3.

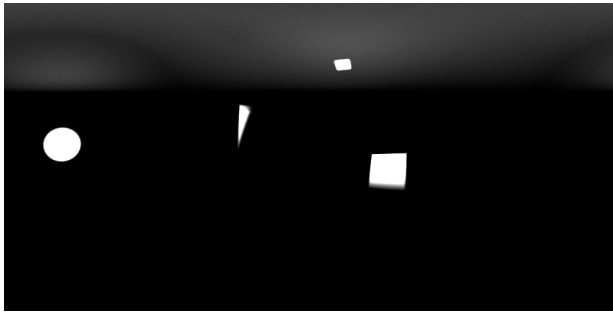


Fig. 10. Artist created IBL used for baseline measurement.

## A APPENDIX

### A.1 ProjectionLoss masks

In Figure 9 we show some example of masks used during calculation of ProjectionLoss defined in Section 3.3.

### A.2 Larger Resolution of Images from our Real-Time App

In Figure 11 we show crops from Figures 1 and 6, for better observation of results from our real-time mobile application.

### A.3 Artist-Created Environment Map

In Figure 10 we show the artist-created environment map used as a baseline in our benchmarking. The artist designed it to satisfy aesthetic and lighting requirements. For lighting, the intensities are selected to make sure the objects were well exposed and that middle gray is retained. The aesthetic brief was to have a “studio lighting” feel with broad area light from behind the camera and from above.

### A.4 Comparisons with recent methods

We made qualitative comparisons to the very recent work of [Srinivasan et al. 2020], that trained and evaluated on synthetic LDR images from InteriorNet [Li et al. 2018] in Figure 12. The authors also provided results from their re-implementation of [LeGendre et al. 2019] and [Song and Funkhouser 2019]. We used the images and results provided as part of their paper and show the comparison to our results in Figure 12. We note that the input to our algorithm was only the incomplete panorama shown in Figure 12(a), while stereo images were used for Srinivasan et al. [2020] (c), and the  $32 \times 32$  sphere image output from LeGendre et al. [2019] was converted

to an equirectangular projection by the authors (d). Furthermore, compared methods were (re) trained by Srinivasan et al. on the same synthetic dataset (InteriorNet [2018]), while our results are using the same network as before, that was trained on public datasets of real-world images discussed in Section 3.1.

Since the network used by Srinivasan et al. was trained on stereo input and LDR ground truth (with reverse gamma), we only make qualitative comparisons for LDR completion/generation of environment maps. We noticed that the predictions made by the algorithm from Srinivasan et al. resembles the (‘unseen’) ground truth textures quite exactly. For example, the window, curtains and wall boundaries match exactly in Figure 12 (c). Given that the input panorama does not have this information, the network should not be able generate textures of an ‘unseen’ test scene with such precision. We are awaiting confirmation from the the authors if the input had more information than shown in the panorama, or the network may have been over fit to a scene used for both training and testing.

Note that our model was trained with images which are aligned with vertical axis being gravity, that is horizon is aligned to the horizontal image axis. This is easily achieved in mobile AR using device pose and orientation, and avoids ambiguity when training a network. The images provided as input (a) have different rotations resulting in some of the artifacts observed. Additionally we observe that the input panoramas are not just masked subset of pixels from the ground truth. The artifacts in the input, such as the blocks and aliasing seen on the left side of first input, could potentially be from reprojection done by Srinivasan et al. , which is carried forward by our results as part of ‘known input’. We manually corrected the above by ‘straightening’ the panoramas (g) and using the input mask to create Corrected Input (h) and show our results from these in row (i). Qualitatively we can observe that our method can produce plausible and perceptually pleasing reflections in these new scenes, even though our model was not trained on the same dataset.

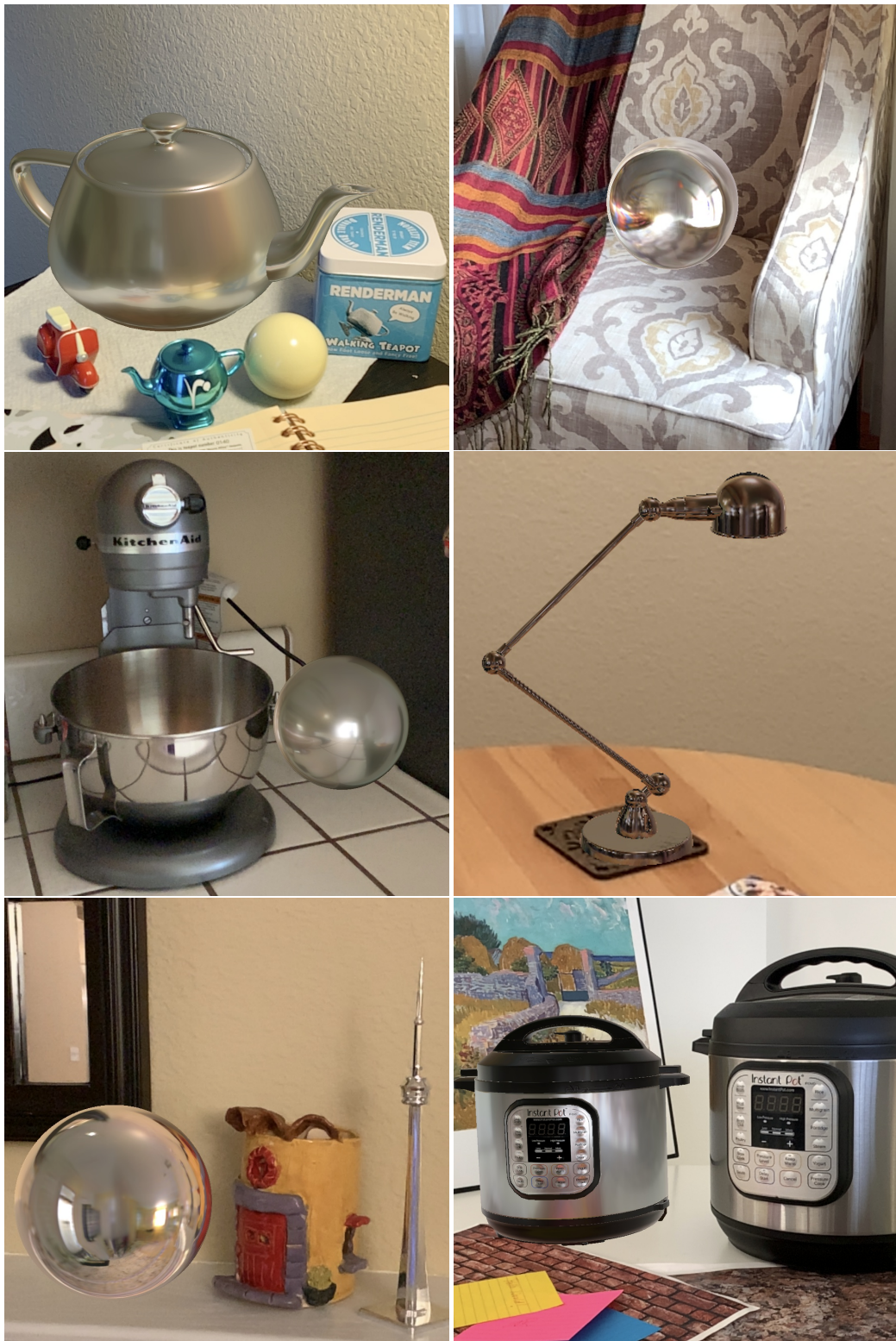


Fig. 11. Croped images from Figures 1 and 6 showing results from our real-time mobile application.

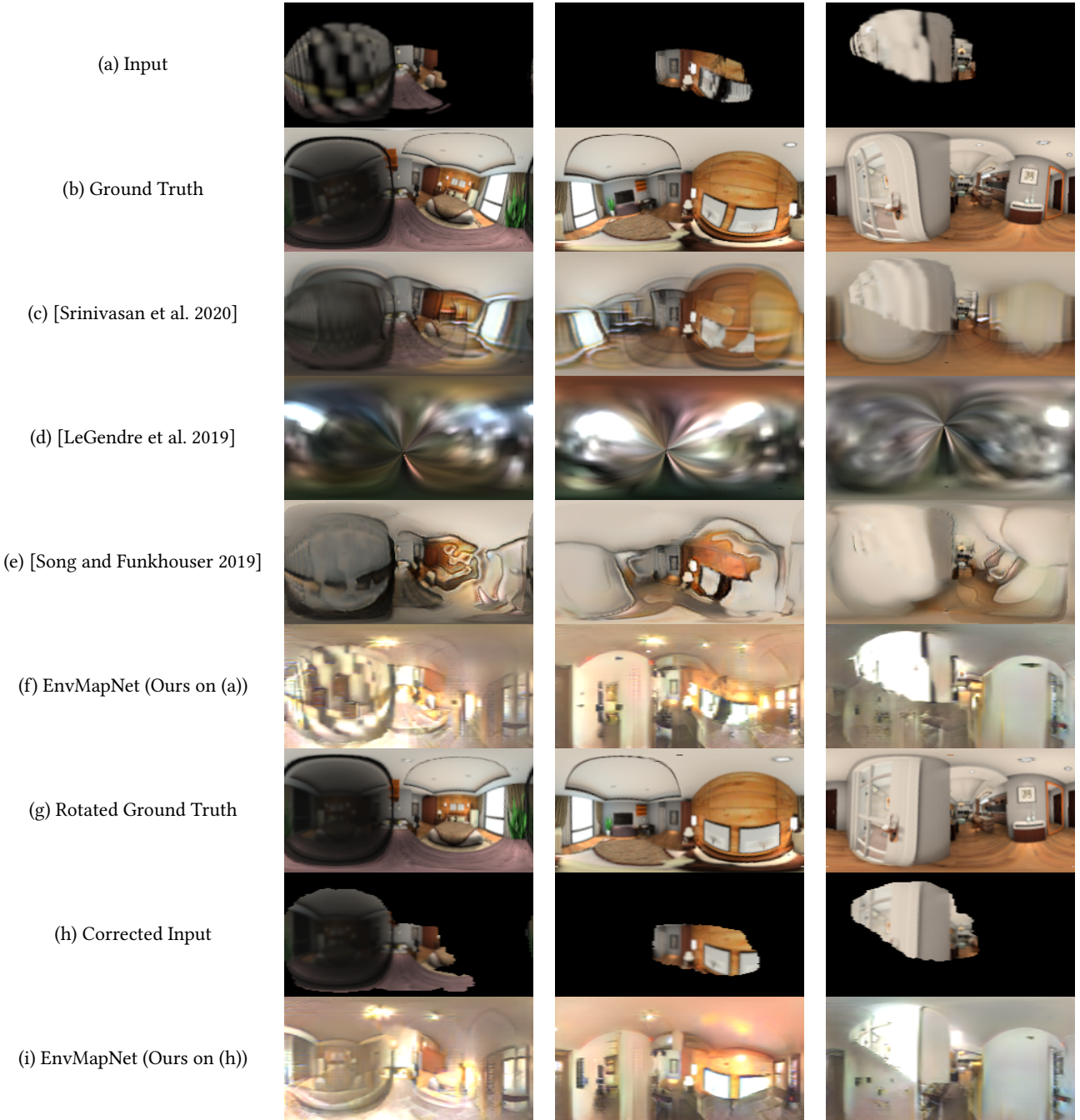


Fig. 12. Comparisons with [Srinivasan et al. 2020]. The input and results are provided by [Srinivasan et al. 2020] and their re-implementation of [LeGendre et al. 2019] and [Song and Funkhouser 2019]. See Appendix A.4 for details.